

Early Stages of Corrosion Phenomena from Impedance Study of Mercury in Aqueous Sodium Chloride

C. V. Krishnan^{1,2,*}, M. Garnett¹ and B. Chu²

¹ Garnett McKeen Lab, Inc., 7 Shirley Street, Bohemia, NY 11716-1735, USA

² Department of Chemistry, Stony Brook University, Stony Brook, NY 11794-3400, USA

*E-mail: ckrishnan@notes.cc.sunysb.edu

Received: 25 July 2008 / Accepted: 9 August 2008 / Published: 8 September 2008

The effects of chloride ion on the electronic properties of the passive film on mercury in aqueous 1.0 M sodium chloride solutions were investigated using admittance and impedance measurements. Impedance loci occurring in the first and second quadrants suggesting tunnel diode behavior and negative differential resistance were observed, for the first time, for mercury in 1.0 M sodium chloride solutions. Admittance measurements indicated an increase in admittance at potentials close to zero followed by a sharp decrease at the beginning of passivation. This maximum becomes sharper at lower frequencies. There is also a slight anodic shift in the maximum with decreasing frequency suggesting the role of solute-water interactions and orientation effects of water near the double layer changeover potential. Mott-Schottky analysis revealed both p-type and n-type semiconduction. Detailed impedance spectra near the double layer crossover potential suggested the high sensitivity of the order of one or two millivolts in the passivation phenomena and the need for careful analysis of this narrow range of potentials for understanding the initial stages of corrosion or passivation phenomena in all metals. The early stages of corrosion can be pinpointed from admittance, Nyquist and Bode plots, and Mott-Schottky plots

Keywords: Double layer, passivity, instantaneous corrosion, negative differential resistance, Mott-Schottky

1. INTRODUCTION

Passivity and passivity breakdown have been studied intensely and numerous for a variety of metals because of all the chlorides in the oceans and its tremendous influence on corrosion [1-10]. Numerous theories and models, such as the point defect model [2], have also been proposed to explain the passivity phenomena in these systems. Chloride is known to be “aggressive” inducing passivity breakdown resulting in different kinds of localized form of corrosion, such as pitting and cracking. It is

suggested that chloride enhances the flux of metal cation vacancies through the passive film resulting in vacancy condensation at the metal/film interface and ensuing passivity breakdown.

We investigated the self-assembly process of large Keplerate type molybdenum clusters of $(\text{NH}_4)_{42}[\text{Mo}^{\text{VI}}_{72}\text{MoV}_{60}\text{O}_{372}(\text{CH}_3\text{COO})_{30}(\text{H}_2\text{O})_{72}] \cdot \text{ca.}300\text{H}_2\text{O} \cdot \text{ca.}10\text{CH}_3\text{COONH}_4$ and found that electrochemical techniques, such as frequency response analysis, could be a useful tool to compliment light scattering and X-ray data [11]. As a prelude, we had carried out electrochemical measurements of simple molybdates at different pH values [12]. Recently we also reported cyclic voltammetry and impedance data for L-cysteine in the absence and presence of counter ions, such as chloride at different pH values, bromide at pH 5.15 and phosphate from buffer at pH 7.03 in order to elucidate solute-solvent interactions and interactions between L-cysteine and counter ions [13]. The L-cysteine study was complimented with an investigation of molybdate-L-cysteine at different pH values [14]. We observed, for the first time, impedance loci occurring in 6 different quadrants in the molybdate-L-cysteine system. From admittance data, we could also assign specific interactions between $\alpha\text{-NH}_3^+$ and $\alpha\text{-COO}^-$ and between Na^+ and sulfhydryl -S^- in L-cysteine. These investigations were needed in order to have a better understanding on the self-assembly process of $\text{Na}_3[\text{Mo}_{154}\text{O}_{462}\text{H}_{14}(\text{H}_2\text{O})_{48}(\text{HO}_2\text{C}(\text{NH}_3^+)\text{HC-CH}_2\text{-S-S-CH}_2\text{-CH}(\text{NH}_3^+)\text{-COO}^-)_{11}] \cdot x \text{H}_2\text{O}$ ($x \approx 250$), another Keplerate type Mo clusters [15]. This interesting structure has multiphilic ligands, such as -NH_3^+ , CO_2^- , CO_2H and -S-S- attached to the inner wall of the cluster through a carboxylate group. Understanding this process will help us synthesize and characterize other ligands for potential medical applications to be incorporated into the Keplerate-type assembly.

Apart from the great interest in aqueous solutions of NaCl whereby one hopes to achieve a better understanding on corrosion, we were also interested in understanding its influence in biological electronic circuits, involving DNA (or RNA or proteins)-salt-water interactions. We reported earlier the results from proteins, collagen and prothrombin, and the profound influence of NaCl on their electronic behavior [16, 17]. While NaCl promoted the electronic behavior of collagen, it was detrimental on prothrombin as evidenced by the occurrence of impedance loci in the first two quadrants, a characteristic of negative differential resistance and probable resonant tunnel diode behavior. We had also reported the admittance and the impedance behavior of aqueous 0.01M KCl, KBr, and KI using a static mercury drop electrode [18]. It was found that the interaction of mercury increased from chloride to bromide to iodide as expected. From Mott-Schottky plots, it was concluded that these systems exhibit both p-type and n-type semi-conduction.

Differential capacity and electrocapillary measurements of potassium halides and/or their mixtures have revealed the nature of specific adsorption and of the double layer [19-21]. These measurements, however, could not distinguish the differences in the structural changes of water at and near the double layer as well as the subtle differences between the cations, such as lithium and cesium.

In our measurements with 0.01M potassium halides, we were puzzled by the high sensitivity of the phase angles at potentials very near the double layer changeover [18]. This behavior prompted us to investigate this aspect further [22]. We chose NaCl instead of KCl because of the abundant nature of NaCl in nature and its involvement in problems related to corrosion. In order to understand our results with 1.0, 0.1 and 0.01M NaCl solutions we had to introduce a new concept, "potential induced water-structure-enforced ion pairing" near the double layer. Our results strongly suggested that one had to

look at minute changes in potential, of the order of one or two millivolts in order to understand the beginning of passivation phenomena. This aspect has been mostly neglected, as far as we know, in the past. Much importance has been given to studies at the passivation potential from polarization curves, of different electrolytes at differing concentrations and pH.

Finally we want to explore the possibility of corrosion prevention or minimization by using the environmentally friendly molybdates, instead of the toxic chromates. The present studies suggest a greater need for looking at transient passivation phenomena as well the need to control counter ions.

We have chosen mercury as the working electrode because all the past electrocapillary measurements for different electrolytes were carried out using mercury. Also it is easier to get a fresh drop each time and thus to minimize surface inhomogeneities. It also offers opportunities to study the influence of surface area more easily because the size of the drop can be easily changed.

2. EXPERIMENTAL PART

An EG & G PARC Model 303A SMDE tri electrode system (mercury working electrode, platinum counter electrode and Ag/AgCl (3.5M KCl, reference electrode) along with Autolab eco chemie was used for cyclic voltammetric and electrochemical impedance measurements at 298 K. Sigma NaCl and distilled water were used for preparation of all solutions. The solutions were purged with N₂ for about 10 minutes before the experiment. Impedance measurements were carried out using about 7 mL solutions in the frequency range 10,000 Hz to 5 mHz. The amplitude of the sinusoidal perturbation signal was 10 mV.

3. RESULTS AND DISCUSSION

3.1. Cyclic voltammetry

These measurements were made for 1.0 M aqueous NaCl solutions at a scan rate of 100 mV/s in the potential range from 0.3 to -1.0V. There was no noticeable activity in the scan range from 0 to -1.0V. The results shown in Figure 1 indicate the interaction of the chloride and consequent passivation of mercury at anodic potentials. The peak potentials observed were 0.041 and 0.105V. There was a slightly higher cathodic current for scan 1 when compared to similar currents for scans 2 and 3. There was no change in the anodic current for all the three scans.

The slight decrease in cathodic current during scans 2 and 3 indicated the influence of the adsorbed species.

We had discussed earlier the cyclic voltammetric results for NaCl concentrations of 1.0, 0.1 and 0.01M and its influence on the passivation of mercury [22]. The lower the concentration of NaCl, the more anodic the potential at which passivation took place.

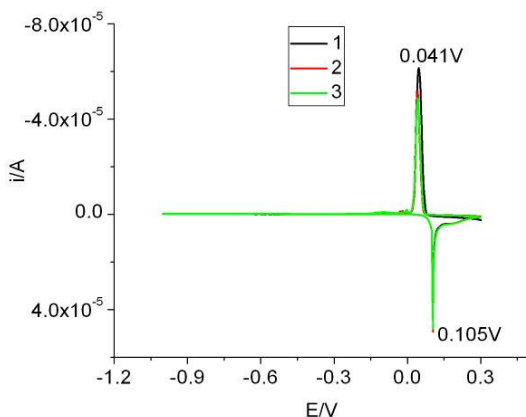


Figure 1. Cyclic voltammetry curves for 1.0 M aqueous sodium chloride. Scan from 0.3 to -1.0V and back. The results of scans 1, 2, and 3 are shown in the figure.

3.2. Frequency Response Analysis

3.2.1. Admittance

The admittance data for 1.0 M aqueous NaCl for 1000 Hz and a comparison of the data for 1000 and 50 Hz are shown in Figures 2a and 2b, respectively. We had reported earlier extensive data for admittance in the frequency range from 10,000 to 50 Hz [22].

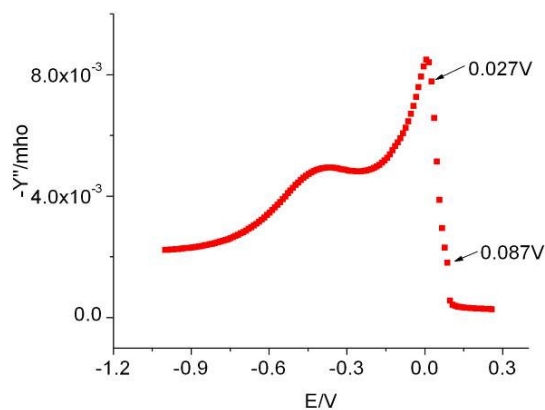


Figure 2a. Admittance of 1.0 M aqueous NaCl, 1000 Hz

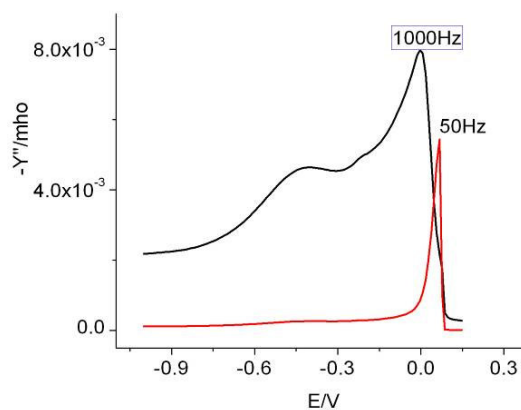


Figure 2b. Admittance of 1.0 M aqueous NaCl 1000 and 50 Hz

Our present investigation has focused on the admittance in the cathodic potential range close to zero. In this region, we observed that as the frequency was decreased, there was a slight anodic shift in the admittance maximum or shoulder (Figure 2b). The admittance increased near potential close to zero volt with decreasing frequency. We also noticed that the maximum in admittance became sharper

with decreasing frequency, as shown in Figure 2b. We should point out that the sharp changes were taking place in the same potential region where cathodic and anodic peaks were observed in the cyclic voltammogram. However, admittance data gave more information regarding solute-solvent interactions near this passivation region. From section 3.2.3, major changes were taking place around 0.08 V where a small shoulder was observed at 1000 Hz.

3.2.2. Differential capacity

In the absence of Faradaic reactions, double layer capacitance was expected to be independent of frequency when obtained from differential capacitance measurements after compensating for ohmic resistance. Figure 3 shows some typical data at 1000 and 100 Hz for 1.0 M NaCl. We did not find any dispersion in the frequency range 1,000 – 50 Hz at cathodic potentials. However, frequency dependence of capacitance was observed for Ag(111) in 0.01 M NaCl [23] and for Cu(111) and Cu(100) in 0.1 M NaOH [24]. These dispersions were often attributed to surface inhomogeneities. Compared to other metal surfaces, mercury is supposed to be defect free and is in agreement with our observations here. A slight dispersion in capacitance with frequency was generally attributed to factors, such as the real surface with fractal character instead of an ideal homogeneous electrode surface, atomic scale inhomogeneities and specific adsorption of anions [23-27]. In the region where Faradaic reaction took place, we observed a slight dispersion.

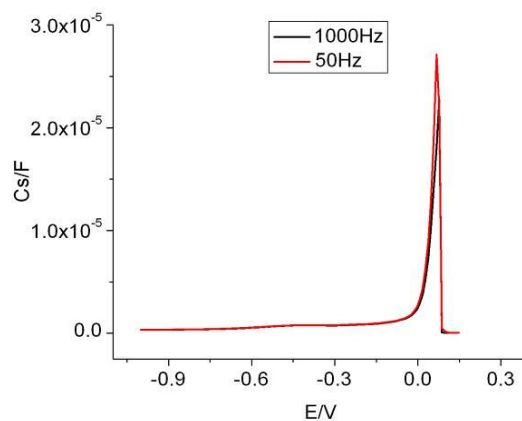


Figure 3. Differential capacitance of 1.0 M aqueous NaCl at 1) 1000 and 2) 100 Hz.

3.2.3. Nyquist and Bode Plots

A typical sequence of Nyquist plots or impedance spectra for 1.0 M NaCl solutions at different potentials are shown in Figures 4 and 5. The potentials chosen corresponded to the transition region, especially the shoulder, as observed in admittance spectra (Figure 2a). The impedance measurement

was carried out immediately after the potential was applied to a fresh Hg drop. The surface area of the mercury drop in each experiment was 0.022 cm^2 .

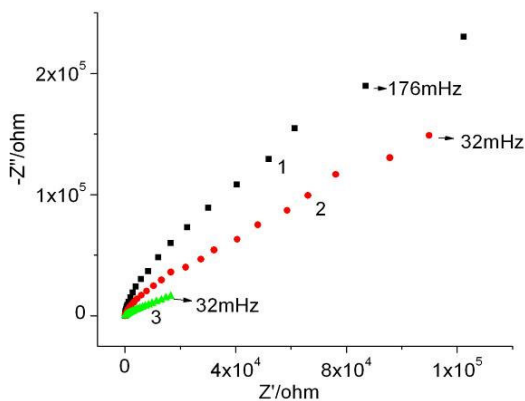


Figure 4a. Nyquist plot for 1.0 M NaCl, 1000 Hz -32 mHz; 1, 0.0 V; 2, 0.04 V; 3, 0.07 V

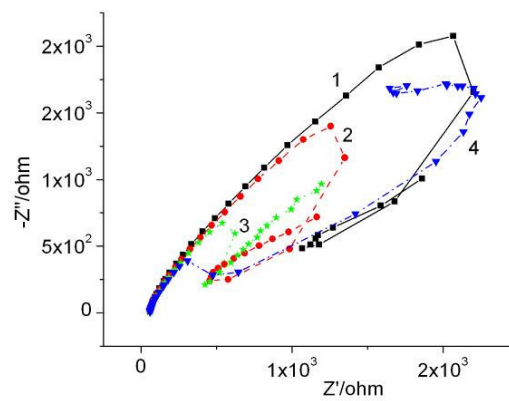


Figure 4b. Nyquist plot for 1.0 M NaCl, 1000 Hz -32 mHz; 1, 0.08 V; 2, 0.081 V; 3, 0.082 V; 4, 0.083 V.

The low frequency data for 0.0 V had to be deleted in order to fit in the same Figure 4a. Also the data for 0.08V is not included in this Figure 4a due to the very low impedance. Similarly the data for 0.084 and 0.085V are not included in Figure 4b due to the much higher impedance. The data for 0.089 and 0.090 V are not included in Figure 5a due to the much higher impedance.

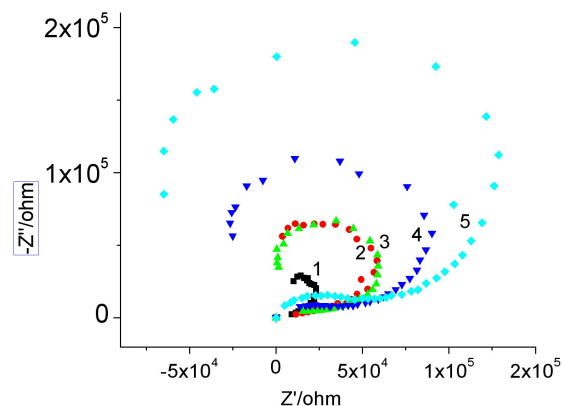


Figure 5a. Nyquist plot for 1.0 M NaCl, 1000 Hz -32 mHz; 1, 0.084 V; 2, 0.085 V; 3, 0.086 V; 4, 0.087 V; 5, 0.088 V

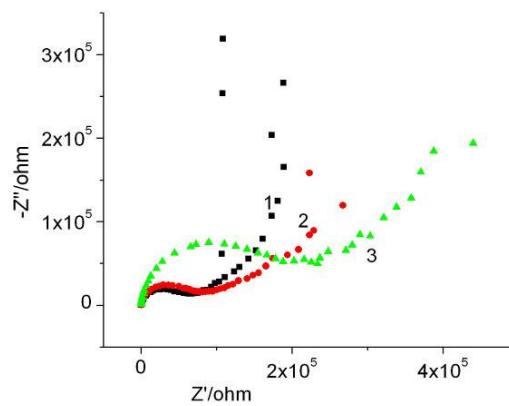


Figure 5b. Nyquist plot for 1.0 M NaCl, 1000 Hz -32 mHz; 1, 0.089 V; 2, 0.090 V; 3, 0.100 V

At potentials below 0.08 V, the impedance was a semicircle. However, the resistance decreased with increasing potential. In the potential region of 0.08 to 0.083 V, the impedance plot of the

semicircle changed direction and formed a loop similar to an inductive loop. Then the loop changed direction again by forming another loop and changed direction with a transition to a negative real part of impedance at low frequencies. It should be interesting to note that all the major changes in impedance were observed between 0.08 and 0.09 V, the region of the shoulder, as observed in admittance measurements (Figure 2). The impedance loci occurring in two quadrants, a characteristic with negative differential resistance, was observed only during the narrow potential range of 0.084-0.088V.

The Bode plots corresponding to the Nyquist plots are given in Figures 6-8. For the purpose of clarity, the phase angle and impedance modulus are shown in separate figures.

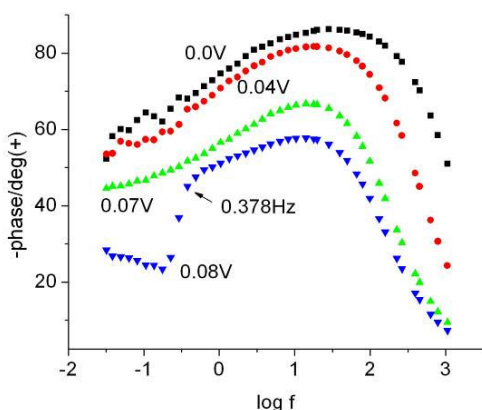


Figure 6a. Bode plot, phase angle for 1.0 M NaCl, 1000 Hz -32 mHz

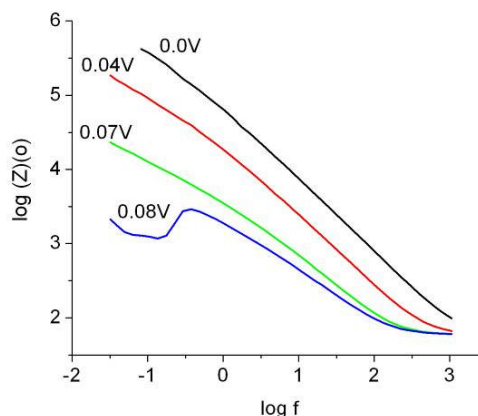


Figure 6b. Bode plot, impedance modulus for 1 M NaCl, 1000 Hz -32 mHz

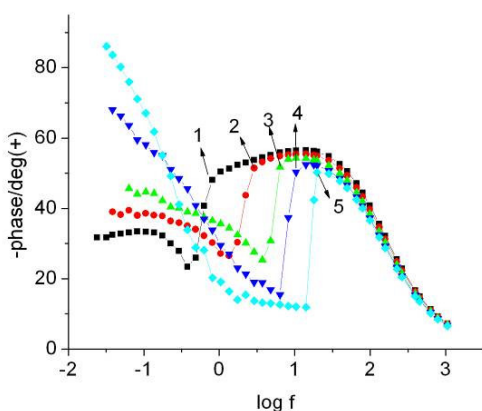


Figure 7a. Bode plot, phase angle for 1.0 M NaCl, 1000 Hz -32 mHz; 1, 0.081 V; 2, 0.082 V; 3, 0.083 V; 4, 0.084 V; 5, 0.085 V. The frequencies at the points indicated by the numbers 1 to 5 are 0.811, 2.90, 3.72, 8.21, and 17.92 Hz

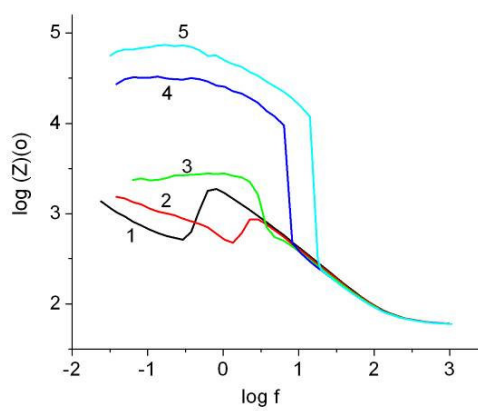


Figure 7b. Bode plot, impedance modulus for 1 M NaCl, 1000 Hz -32 mHz; 1, 0.081 V; 2, 0.082 V; 3, 0.083 V; 4, 0.084 V; 5, 0.085 V

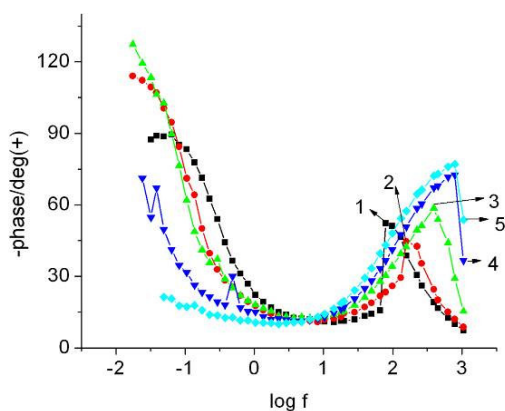


Figure 8a. Bode plot, phase angle for 1.0 M NaCl, 1000 Hz -32 mHz; 1, 0.086 V; 2, 0.087 V; 3, 0.088 V; 4, 0.089 V; 5, 0.090 V

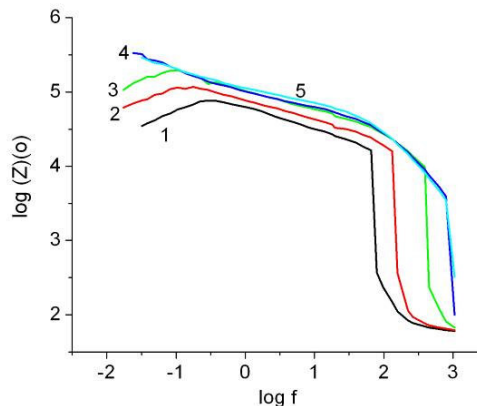


Figure 8b. Bode plot, impedance modulus for 1.0 M NaCl, 1000 Hz - 32 mHz; 1, 0.086 V; 2, 0.087 V; 3, 0.088 V; 4, 0.089 V; 5, 0.090 V

At low frequencies, the dramatic change in the phase angle around - 45 degrees as observed in Figure 7a and the curving upward of the impedance modulus (Figure 7b) were somewhat similar to the behavior observed for type 304 stainless steel in aqueous NaCl [28]. This behavior had been attributed to the diffusion reaction taking place at the passivated electrode [29].

Using the Bode plots, Warburg diffusion coefficients σ were calculated at $f = 1$:

$$\log(Z)(o) = \log \sigma \Pi^{-1/2} - \frac{1}{2} \log f$$

For type 304 stainless steel σ was found to increase with increasing potential at a given Cl⁻ concentration. This was attributed to the thicker and more abundant salt films on the electrode at more anodic potentials. At a given potential, σ was found to decrease with decreasing Cl⁻ concentration. This was attributed to insufficient Cl⁻ ions at the channel between the sites and the bulk electrolyte in spite of the fact that the sites on the surface were activated at lower potentials. Under these conditions, the metastable pits could not be maintained for propagation. Therefore, these sites died out by repassivation at the nucleation stage [29].

In the above experiments with type 304 stainless steel at varying concentrations of aqueous NaCl, the potential variation was in steps of 25 mV. Also in most corrosion studies, not enough attention has been paid to the influence of the bulk electrolyte behavior at or near the double layer. We propose to suggest the following alternative and complimentary explanation for consideration in all studies related to corrosion phenomena.

The relationship between the three dimensional solution concentrations in the bulk and the two-dimensional ionic concentrations at an electrode interface is given by the equation [30]:

$$\begin{aligned} C_i &= \check{I}_i^{3/2} N^{1/2} 1000 \text{ mol dm}^{-3} \\ &= (q_i/F)^{3/2} N^{1/2} 1000 \text{ mol dm}^{-3} \end{aligned}$$

where $\check{\Gamma}_i = 2$ -dimensional surface concentration in mol cm⁻² of an ion of type i in the interphase; $C_i =$ the equivalent 3-dimensional concentration; q_i is the adsorbed ion charge in the inner layer, C m⁻²; $N =$ Avogadro's number. From this, it is seen that for $\pm q_i = 0.05$, $\check{\Gamma}_i = 5.19$ and $C_i = 0.50$. It is seen that the 2-dimensional surface concentration is about 10 times higher than the bulk 3-dimensional concentration. We should keep this in mind when we consider the interionic effects as well as the co-sphere overlap effects.

We have discussed in great detail the influence of various types of ion pairs in explaining the admittance data of simple electrolytes at various concentrations. In this process we have introduced a new concept, "potential induced water-structure-enforced ion pairing" [22]. This supposition was reinforced in our studies of L-cysteine and molybdate-L-cysteine where we could pinpoint specific ionic interactions as well as solute-solvent interactions [13, 14]. If the passivation potential were near the region where there was a considerable change in the orientation of water molecules near the double layer, then it would be possible, at or near the double layer, to have a potential induced water-structure-enforced ion pair formation between the ions of the bulk electrolyte, either directly or mediated by water molecules. If this process were to occur, it would become easier for penetration of the electrolyte.

In most studies related to corrosion or passivation phenomena, the common practice was to passivate the metal for an extended period of time and then to look at the impedance spectra. We believe, it is advisable, whenever possible, to investigate initial stages of passivation phenomena because these data are loaded with rich information about the interactions at the electrode and at or near the double layer.

3.2.4. Mott-Schottky Plots

The space charge region of the semiconductive passive films, produced by polarization of the metal at various potentials, is often characterized by carefully evaluating the capacitance. These passive films on many metals and alloys exhibit properties of an inner p-type oxide layer and an outer

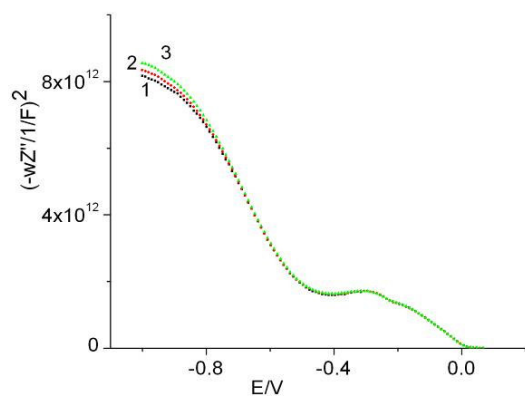


Figure 9a. Mott-Schottky plot for 1.0 M aqueous NaCl; 1, 10,000 Hz; 2, 5,000 Hz; 3, 1,000 Hz

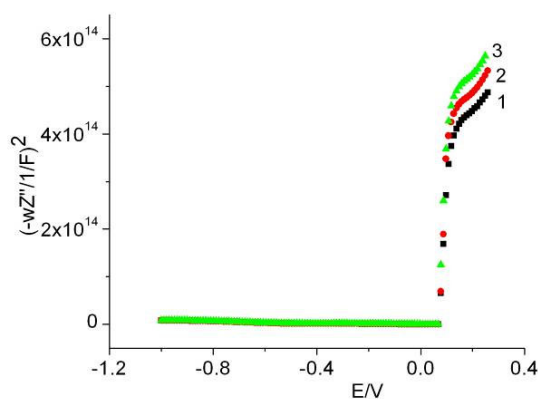


Figure 9b. Mott-Schottky plot for 1.0 M aqueous NaCl; 1, 10,000 Hz; 2, 5,000 Hz; 3, 1,000 Hz

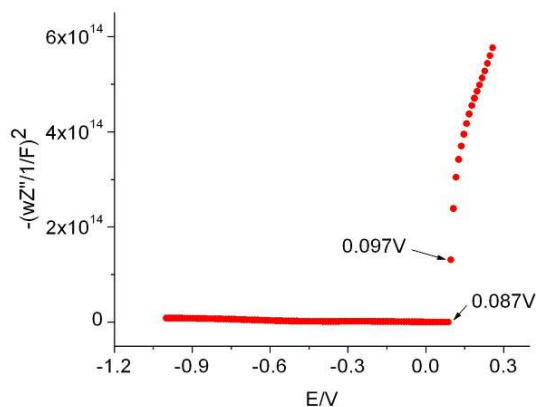


Figure 9c. Mott-Schottky plot for 1.0 M aqueous NaCl; 1, 1000 Hz

n-type hydroxide layer with a p-n heterojunction [31, 32]. From the measurements of the imaginary part of the impedance (Z'') as a function of the applied potential, the corresponding capacitance of the space charge layer, C , was obtained from

$$C = -1/(\omega Z'')$$

It is assumed that the capacitance of the Helmholtz layer is large compared to that of the space charge region. Then the characteristic space charge capacitance of these semiconducting films obeys the Mott-Schottky relationship that connects C of a p-type semiconductor and the electrode potential E :

$$C^{-2} = -[2/(q\epsilon \epsilon_0 N_A)] (E - E_{FB} + kT/q)$$

where ϵ is the vacuum permittivity (8.85×10^{-14} F/cm), ϵ_0 the dielectric constant of the specimen, q the electron charge (1.602×10^{-19} Coulomb), k the Boltzmann constant (1.38×10^{-23} J/K), T the absolute temperature, N_A the acceptor density, and E_{FB} the flat band potential. The intercept on the potential axis gives the flat band potential. The slope is inversely proportional to the doping concentration and can be obtained provided the dielectric constant of the passive film is known.

Some typical Mott-Schottky plots for 1.0 M NaCl are shown in Figure 9. In order to see the comparative behavior more clearly, the data are truncated at the more positive potentials in Figure 9a. We had observed different flat band potentials for Cl^- , Br^- , and I^- [18]. We could, therefore, suggest that it was not just the oxide and hydroxide layers responsible for this observed phenomena. Instead the highly insoluble mercurous ion chloride complex might be involved in the formation of the film. Figure 9c points out the narrow transition region where spectacular phase behavior and impedance loci with negative differential resistance were observed.

For many metals, the growth of the oxide film is due to the migration of both the cation and O^{2-} ion through the film under the influence of the high electric field of about a million volts per cm. In the present case, it might well be due to the formation of a mercurous halide film formation and

subsequent growth of this film instead of the oxide film and oxide growth and could be similar to the well known substitutions of other cations and anions taking place in aluminum alloys.

3.3. Stability of Experimental Data

We have checked the reproducibility of the data in different ways. For example the reproducibility of the admittance data is shown in Figure 10a. These are three sets of data from three different days. The other is the reproducibility of the impedance data showing impedance loci in the

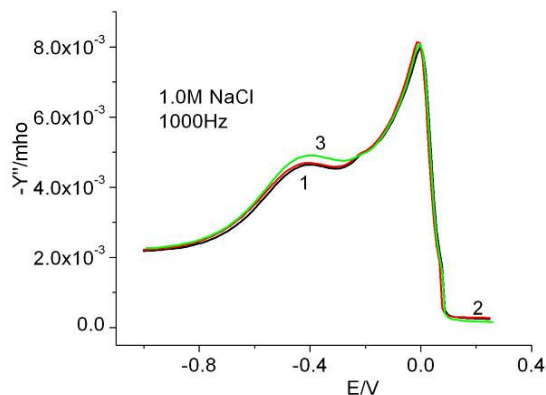


Figure 10a. Admittance data for 1.0 M NaCl at 1000 Hz obtained from three different days from solutions of different preparations

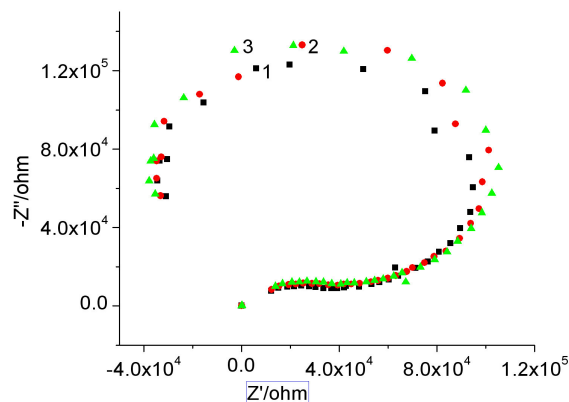


Figure 10b. Reproducibility of impedance data for 1.0 M NaCl at 0.087 V, 1000-0.018 Hz, Nyquist plot, 3 sets of data

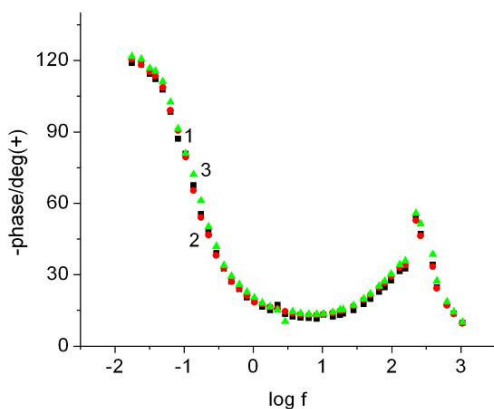


Figure 10c. Reproducibility of impedance data for 1.0 M NaCl at 0.087 V, 1000- 0.018 Hz Bode plot, phase angle. Three sets of data

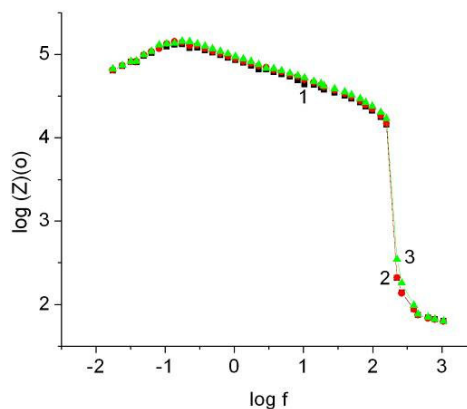


Figure 10d. Reproducibility of impedance data for 1.0 M NaCl at 0.087 V, 1000- 0.018 Hz Bode plot, modulus of impedance, three sets of data

first and second quadrants, and are shown in Figure 10b. The corresponding Bode plot data for phase angle and modulus of impedance are shown in Figures 10c and 10d. Considering the complexity of the system, the reproducibility of the data is excellent. We had pointed out earlier that one could manipulate the visual observation of the scatter by carefully selecting the type of data for reproducibility [18]. The purpose of our experiment was to demonstrate that the impedance loci occurring in the first and second quadrant was real, reproducible, and was very sensitive to subtle changes in the applied potential.

3.4. Surface Area

Compared to other working electrodes used in corrosion studies, it is fairly easy to have a fresh clean surface for mercury. Also the surface area of the mercury can be easily controlled by use of the dispense button in the 303A electrode system. We have studied the influence of surface area on the electronic properties of the mercury-aqueous sodium chloride and the results are shown in Figure 11.

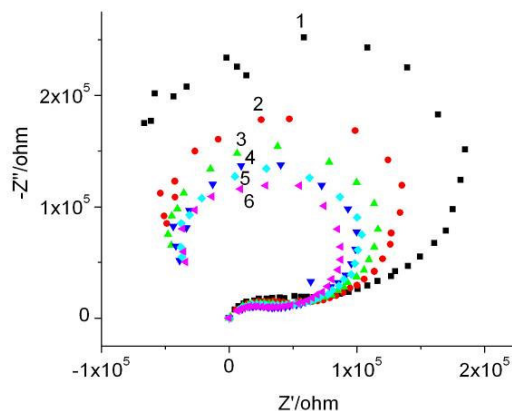


Figure 11. Influence of surface area on the impedance of 1.0 M NaCl at 0.087 V. Surface area in cm^2 , 1) 0.011 2) 0.017 3) 0.022 4) 0.027 5) 0.031 6) 0.035

As expected the impedance became less and less with increased surface area. It would appear that the electronic process became more efficient with increasing surface area.

4. Mercury(I) and mercury(II) complexes

In considering the various processes taking place at the mercury electrode during the passivation process, one has to consider the following interactions.

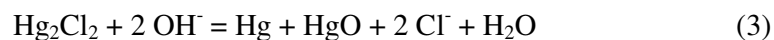
The solubility of Hg_2Cl_2 is 2×10^{-4} g/100g water at 25 °C with a (log) solubility product constant of -17.88 [33]. The reported standard electrode potential for the reaction:



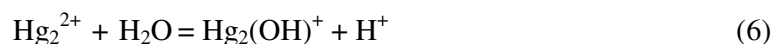
is 0.2682 V [35]. The equilibrium constant for the disproportionation reaction:



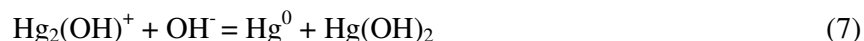
is 1.15×10^{-2} with a potential of -0.1150 V at 25°C [33]. Disproportionation can also occur, especially in basic medium, by the following reaction:



Hydrolysis of both Hg^{2+} and Hg_2^{2+} should also be considered.



with hydrolysis constants of $10^{-3.5}$, $10^{-2.7}$, and 10^{-5} for equations 4, 5, and 6 respectively. These hydrolysis constants suggest greater acidity for Hg^{2+} solutions than for Hg_2^{2+} solutions. In the presence of OH^- , $\text{Hg}_2(\text{OH})^+$ is known to disproportionate [34] by the reaction



The activated complex for the above reaction has been postulated as $[\text{HO-Hg-Hg-OH}]$ and $[\text{Hg-Hg}(\text{OH})_2]$ [34]. Reaction 2 is shifted to the right by the presence of ions such as OH^- , CN^- and Cl^- . In most common corrosion processes in metals, reactions similar to equations 4 and 5 are important while equations 1, 2, 3, 6, and 7 are relevant only for mercury. The interaction of $\text{Hg}(\text{OH})^+$, $\text{Hg}_2(\text{OH})^+$, Hg_2^{2+} and Hg^{2+} with Cl^- also cannot be neglected. For example, known mercury(I) oxychlorides include $2\text{HgO} \cdot \text{Hg}_2\text{Cl}_2$ and $2\text{Hg}_2\text{Cl}_2 \cdot \text{Hg}_2\text{O}$.

The complicated phase change behavior and the impedance behavior as well as their extreme sensitivity to minute variations in potential can be understood from the involvement of these different processes.

4. CONCLUSIONS

The effects of chloride ion on the electronic properties of the passive film on mercury in aqueous 1.0 M sodium chloride solutions were investigated using admittance and impedance measurements. Impedance loci occurring in the first and second quadrants suggesting tunnel diode

behavior and negative differential resistance were observed for the first time for mercury in 1.0 M sodium chloride solutions.

Admittance measurements indicated an increase in admittance at potentials close to zero followed by a sharp decrease at the beginning of passivation. This maximum becomes sharper at lower frequencies. There is also a slight anodic shift in the maximum with decreasing frequencies suggesting the role of solute-water interactions and orientation effects of water near the double layer changeover potential. Mott-Schottky analysis revealed both p-type and n-type semiconduction. Detailed impedance spectra near the double layer crossover potential suggested the high sensitivity of the order of one or two millivolts in the corrosion or passivation phenomena and the need for careful analysis of this narrow range of potential for understanding the initial stages of passivation phenomena in all metals. This region of passivation can be pinpointed from admittance, Bode plots and Mott-Schottky plots.

ACKNOWLEDGEMENT

Ben Chu acknowledges financial support of this work provided by the Basic Energy Sciences, Department of Energy (DEFG0286ER45237)

References

1. S-J. Ahn, H-S. Kwon, D. D. Macdonald, *J. Electrochem. Soc.*, 152 (2005) B482
2. D. D. Macdonald, *Pure Appl. Chem.*, 71 (1999) 951
3. D. D. Macdonald, *J. Electrochem. Soc.*, 139 (1992) 3434
4. C. Y. Chao, L. F. Lin, D. D. Macdonald, *J. Electrochem. Soc.*, 128 (1981) 1187
5. L. F. Lin, C. Y. Chao, D. D. Macdonald, *J. Electrochem. Soc.*, 129 (1981) 1194
6. D. D. Macdonald, M. Urquidi-Macdonald, *J. Electrochem. Soc.*, 137 (1990) 2395
7. N. Sato, *Passivity of Metals*, R. P. Frankenthal and J. Kruger, Editors, The Electrochemical Society, Princeton, N.J. (1978)
8. D. K. Merl, P. Panjan, M. Čekada, M. Maček, *Electrochimica Acta*, 49 (2004) 1527
9. L.A.S. Ries, M.D.C. Belo, M.G.S. Ferreira, I.L. Muller, *Corrosion Science*, 50 (2008) 676
10. C. Liu, Q. Bi, A. Leyland, A. Matthews, *Corrosion Science*, 45 (2003) 1243
11. C. V. Krishnan, Q. Li, B. Chu, *Electrochimica Acta*, 53 (2007) 975
12. C.V. Krishnan, M. Garnett, B. Hsiao, B. Chu, *Int. J. Electrochem. Sci.*, 2 (2007) 29
13. C.V. Krishnan, M. Garnett, B. Chu, *Int. J. Electrochem. Sci.*, 3 (2008) 854
14. C.V. Krishnan, M. Garnett, B. Chu, *Int. J. Electrochem. Sci.*, 3 (2008) 873
15. A. Muller, S.K. Das, C. Kuhlmann, H. Bogge, M. Schmidtman, E. Diemann, E. Krickemeyer, J. Hormes, H. Modrow, M. Schindler, *Chem. Commun.*, 655 (2001)
16. C. V. Krishnan, M. Garnett, *Int. J. Electrochem. Sci.*, 1 (2006) 215
17. C. V. Krishnan, M. Garnett, *Int. J. Electrochem. Sci.*, 1 (2006) 283
18. C. V. Krishnan, M. Garnett, *Electrochimica Acta*, 51 (2006) 1541
19. D. C. Grahame, R. Parsons, *J. Am. Chem. Soc.*, 83 (1961) 1291
20. D. C. Grahame, *J. Am. Chem. Soc.*, 80 (1958) 4201
21. R. Payne, *Trans. Faraday Soc.*, 64 (1968) 1638
22. C.V. Krishnan, M. Garnett, B. Chu, *Int. J. Electrochem. Sci.*, 2 (2007) 958
23. V. D. Jovic, B. M. Jovic, *J. Electroanal. Chem.*, 54 (2003) 1
24. V. D. Jovic, B. M. Jovic, *J. Electroanal. Chem.*, 54 (2003) 13
25. Z. Kerner, T. Pajkossy, *Electrochimica Acta*, 46 (2000) 207

26. J.R. Macdonald, C.A. Barlow, Jr., *J. Chem. Phys.* 36 (1962) 3062
27. J.R. Macdonald, *J. Chem. Phys.*, 22 (1954) 1857
28. T. Hong, M. Nagumo, *Corrosion Science*, 39 (1997) 285
29. T. Hong, G.W. Walter, M. Nagumo, *Corrosion Science*, 38 (1996) 1525
30. B.E. Conway, *J. Electroanal. Chem.*, 123 (1981) 81
31. H. Tsuchiya, S. Fujimoto, T. Shibata, *J. Electrochem. Soc.*, 151 (2004) B39 and references therein
32. D.S. Kong, S.H.Chen, C. Wang, W. Yang, *Corrosion Science*, 45 (2003) 747 and references therein
33. J. C. Bailar Jr., H.J. Emeleus, R. Nyholm, A.F.T. Dickenson, *Comprehensive Inorganic Chemistry*, Pergamon Press, Vol.3 (1973) 287
34. I. Sanemasa, *Inorg. Chem.*, 16 (1977) 2786